

Strain localization and yielding dynamics in disordered collagen networks

Swarnadeep Bakshi^a, Vaisakh VM^{a,b}, Ritwick Sarkar^a, and Sayantan Majumdar^{a*}

^a*Soft Condensed Matter Group, Raman Research Institute, Bengaluru 560080, India*

^b*Department of Physics, HKUST, Clear Water Bay, Hong Kong*

(Dated: December 23, 2024)

Collagen is the most abundant extracellular-matrix protein in mammals and the main structural and load-bearing element of connective tissues. Collagen networks show remarkable strain-stiffening properties which tune the mechanical functions of tissues and regulate cell behaviours. Linear and non-linear mechanical properties of in-vitro disordered collagen networks have been widely studied using rheology for a range of self-assembly conditions in recent years. However, a one to one correlation between the onset of macroscopic network failure and local deformations inside the sample is yet to be established in these systems. Here, using shear rheology and in-situ high-resolution boundary imaging, we study the yielding dynamics of in-vitro reconstituted networks of uncrosslinked type-I collagen. We find that in the non-linear regime, the differential shear modulus (K) of the network initially increases with applied strain and then begins to drop as the network starts to yield beyond a critical strain (yield strain). Measurement of the local velocity profile using colloidal tracer particles reveals that beyond the peak of K , strong strain-localization and slippage between the network and the rheometer plate sets in that eventually leads to a detachment. We generalize this observation for a range of collagen concentrations, applied strain ramp rates, as well as different network architectures obtained by varying the polymerization temperature. Furthermore, by fitting the stress vs strain data with a continuum affine network model, we map out a state diagram showing the dependence of yield-stain and -stress on the reduced persistence length and mesh size of the network. Our findings can have broad implications in tissue engineering, particularly, in designing highly resilient biological scaffolds.

I. INTRODUCTION

Biopolymer networks, the major structural component of intra- and extracellular environment in animal body, show strikingly different mechanical properties compared to synthetic polymer gels [1–8]. Properties like non-linear strain stiffening, negative normal stress in biopolymers are related to the ‘semi-flexibility’ of the filaments as indicated by their relatively high bending rigidity (κ). In polymeric system, the filament rigidity is generally expressed in terms of thermal persistence length ($l_p = \frac{\kappa}{k_B T}$) that indicates how tangent-tangent angular correlation decays along the filament due to thermal fluctuations. For biopolymers, l_p is significantly larger than that for the synthetic polymers, yet, much smaller compared to a rigid rod. This indicates that despite of their rigidity, biopolymers show significant thermal bending fluctuations [8–10].

*smajumdar@rri.res.in

Type-I collagen is the most abundant protein in the extracellular matrix (ECM) of mammalian cells. Besides providing a scaffold for connective tissues, the mechanical and structural properties of ECM governs crucial cellular functions like cell proliferation, adhesion, migration, wound-healing, signaling etc [11–14]. Abnormalities in ECM stiffness gives rise to various pathological conditions [15, 16].

To better understand the effect of linear and non-linear mechanics on various cellular and tissue functionalities, in-vitro reconstituted assemblies of disordered isotropic collagen networks have become very popular in recent years, particularly, in the context of bio-physics, mechano-biology and tissue engineering [17–19]. Such studies consider both simple shear [20, 21] and extensional deformations [22]. Non-linear mechanics of collagen is complex and highly architecture dependent [23]. Collagen networks with similar linear moduli can have widely different non-linear strain stiffening response [24]. The complexity mainly arises from the presence of hierarchical length scales in the system. Entropic elasticity of individual filaments, non-affine deformations, network heterogeneity, stress induced changes in network architecture contribute to the non-linear mechanics in these systems. Interestingly, collagen networks can show stability and finite elasticity for the average local network connectivity $\langle z \rangle$ varying approximately between 3 and 4 which is well below the isostaticity ($\langle z \rangle = 6$ in three dimension) as predicted by Maxwell criterion [25]. Theoretical models demonstrate that bending rigidity of filaments stabilizes such sub-isostatic networks and strain stiffening originates from a bending to a stretching dominated response of the individual filaments/bundles [4, 26, 27]. Continuum unit-cell models (e.g. 3-Chain and 8-Chain Models) of semi-flexible filaments, provide compact analytical expressions effectively describing the non-linear strain stiffening in different biopolymer networks [28, 29].

Rheology and in-situ microscopy techniques like, confocal fluorescence (CFM), confocal reflectance (CRM) and boundary stress microscopy (BSM) provide important insight into the correlation of visco-elasticity, network deformation, failure and stress heterogeneity with the local network structure in these systems [30–32]. Stress relaxation in these systems strongly influenced by the magnitude of applied strain [20]. Similar to other biopolymers, non-linear mechanics of collagen networks also demonstrates striking hysteric effects [33–35].

Although, non-linear strain stiffening in disordered isotropic collagen networks has been extensively studied, much less attention has been paid to the dynamics of yielding and network failure. It is found that network architecture affects the magnitude of yield strain in collagen. Networks polymerized at higher temperature having finer fibrils with smaller pore sizes show a much larger yield strain compared to that corresponding to more bundled networks obtained at lower polymerization temperatures [23, 24]. Non-linear mechanics and yielding in these systems also show interesting system-size dependence over the length scales much larger than the network mesh size [36]. A very recent study attempts to correlate the fracture strain with the local connectivity and plasticity of the collagen network using rheology and in-situ CFM. They directly probe the network failure over the length scales of single filaments to a few mesh size [31].

Despite of these studies, a direct correlation between the onset of bulk network failure and microscopic deformations still needs to be established. Moreover, in all the studies probing change in network structure using CFM and CRM in conjugation with rheological measurements, the imaging is done in the flow-vorticity plane compatible

with standard microscopy set-up. Particularly, high resolution imaging in the flow-gradient plane is difficult due to the presence of air-sample interface in a plate-plate or cone-plate geometries used for the rheology measurements. Interestingly, the possibility of strain localization in the flow-gradient plane has been speculated in the context of system-size dependent stiffening and yielding in collagen networks [36]. However, to our knowledge, in-situ strain distribution over mesoscopic to macroscopic length scales in flow-gradient plane has not been explored in these systems.

Here, we study non-linear strain stiffening and yielding behaviour in uncrosslinked type-I collagen networks using rheology and in-situ boundary imaging over a range of concentrations and polymerization temperatures. We find that the network softening or yielding starts well below the breaking/rupture strain. We also observe that high strain accumulates in the sample near the shearing boundaries when the applied strain crosses the yield strain. Such localized strain initiates a slippage between the network and the rheometer plate eventually leading to a detachment. Furthermore, fitting the stress-strain curves with a unit cell based network model for affine deformations, we map out a state diagram connecting the yielding behavior with the reduced persistence length and mesh-size of the network.

II. RESULTS AND DISCUSSIONS

We reconstitute networks of Type-I collagen starting from collagen monomers. Collagen monomers are formed by triple-helical polypeptides of length ≈ 300 nm and width ≈ 1.5 nm [37, 38]. Under suitable buffer condition (Materials and Methods) the polymerization process takes place giving rise to space-filling collagen networks. Polymerization time and network architecture strongly depends on the parameters like temperature [39–41], pH [42–44], ionic concentration [44, 45]. The typical network architecture for two different polymerization temperatures are shown in Fig. 1(a) and (b). At 4°C, the network is very heterogeneous with thick parallel bundles, whereas, more homogeneous network with finer fibrils are observed at 25°C. The distributions of fibril/bundle diameter for different temperatures are obtained from the freeze fracture SEM data (sample size: $N \sim 400$) is shown in Fig. 1(c). We find that over the temperature (T) range of 4°C - 35°C, both the mean and standard deviation filament diameter decreases with increasing temperature, as also reported in earlier studies [23, 39, 46].

Rheology measurements are carried out on a MCR-702 stress-controlled rheometer (Anton Paar, Graz, Austria) using cone-plate geometry having rough sand-blasted surfaces (Materials and Methods). Such rough surfaces minimize wall-slippage of the sample under shear. The polymerization process of collagen is monitored by applying a small oscillatory shear strain (amplitude $\gamma_0 = 2\%$, frequency $f = 0.5$ Hz) and measuring the linear visco-elastic moduli G' and G'' as a function of time. After an initial increase, G' and G'' reaches a plateau value (Fig. S1), indicating that the network is polymerized. We carry out the rheology measurements over a concentration (ϕ) range of 1 mg/ml - 3 mg/ml. In all cases, we find that over a wide range of frequency $G'(f)$ is much larger than $G''(f)$ (Fig. S2), indicating that the networks behave like a visco-elastic solid. To probe the response of the network as a function of strain, we apply a constant strain ramp rate $\dot{\gamma} = 1\%/s$ on the network and measure the stress response. We show the variation of shear stress (σ) and differential shear modulus $K = \frac{d\sigma}{d\gamma}$ as a function of γ (Fig. 1(d)) for $\phi = 2$ mg/ml and T = 35°C. We find that after a mild strain-weakening regime, K increases rapidly beyond an onset strain γ_o indicating the non-linear strain stiffening of the network, when the shear modulus of the network increases with increasing strain. At larger strain values, K reaches a maximum before starting to drop beyond γ_y , the yield-strain of the network,

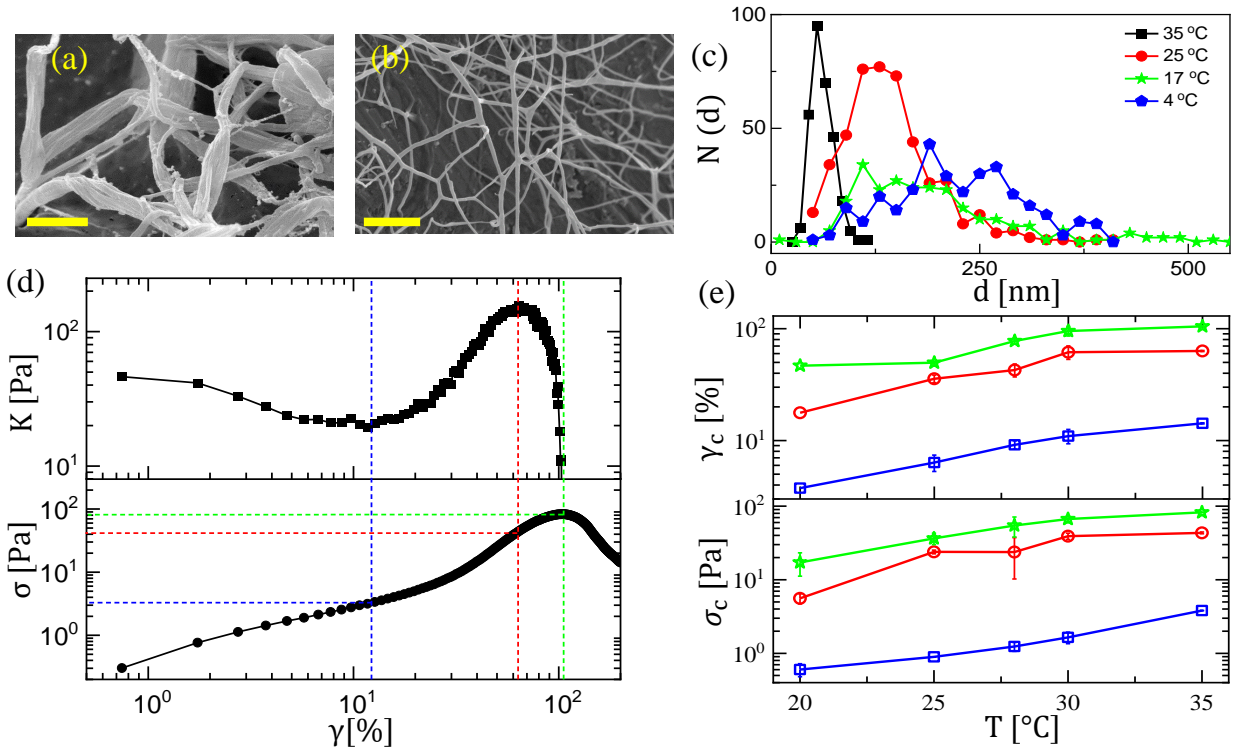


Figure 1: Freeze-fracture SEM image of collagen polymerized at (a) 4°C (Scale = 1 μm) and (b) 25°C (Scale = 2 μm). (c) Bundle fibril diameter distribution. For Fig. 1(a),(b) and (c), the collagen concentration $\phi = 1 \text{ mg/ml}$. (d) Variation of differential shear modulus (top panel) and stress (bottom panel) with applied strain for polymerization temperature $T = 35^\circ\text{C}$. Critical stress and strain points corresponding to the onset, yield and breaking are marked with the dashed lines. (e) Variation of critical strain and stress as a function of polymerization temperature (squares: onset stress/strain, circles: yield stress/strain and stars: breaking stress/strain). Error bars represent standard deviations for two independent measurements. For Fig. 1(d) and (e) the collagen concentration $\phi = 2 \text{ mg/ml}$.

indicating a network weakening under large strain. Interestingly, the peak stress is reached at a higher strain value compared to γ_y . We define the strain value at which the stress reaches the peak as the breaking/rupture strain γ_b for the network. Beyond γ_b the stress weakening starts. Mathematically, $\frac{d^2\sigma}{d\gamma^2}|_{\gamma_y} = 0$ and $\frac{d\sigma}{d\gamma}|_{\gamma_b} = 0$ defines the yielding and breaking points of the network, respectively. From Fig. 1(d) and (e) we note that $\gamma_y \approx 50\%$ whereas, $\gamma_b \approx 100\%$. This points out that for disordered collagen networks yielding is a gradual process rather than an abrupt one. We show the variation of γ_o , γ_y and γ_b and the corresponding stress values (σ_o , σ_y , σ_b) as a function of polymerization temperature in Fig. 1(e) (top and bottom panels). We find that both the critical strain and stress values increase with increasing temperature. Similar trends are also observed for $\phi = 1 \text{ mg/ml}$ and 3 mg/ml (Fig. S3). For temperatures below 20°C , we observe condensation of small water droplets on the rheometer plates. This can change the moment of inertia of the shearing plates and introduce measurement artifacts. Thus, for rheology measurements we do not probe any temperature below 20°C .

To get a deeper insight into the yielding behaviour of collagen networks, we map out the spatio-temporal evolution of the velocity field in the sample using particle imaging velocimetry (PIV) technique. We illuminate the sample using a LED light source (Dolan-Jenner Industries) and image the diffused scattering from the sample boundaries in the flow-gradient plane using a digital camera (Lumenera) fitted with a 5X long working distance objective (Mitutoyo). We do not get any appreciable scattering from the pure collagen and the sample appears almost transparent. We put

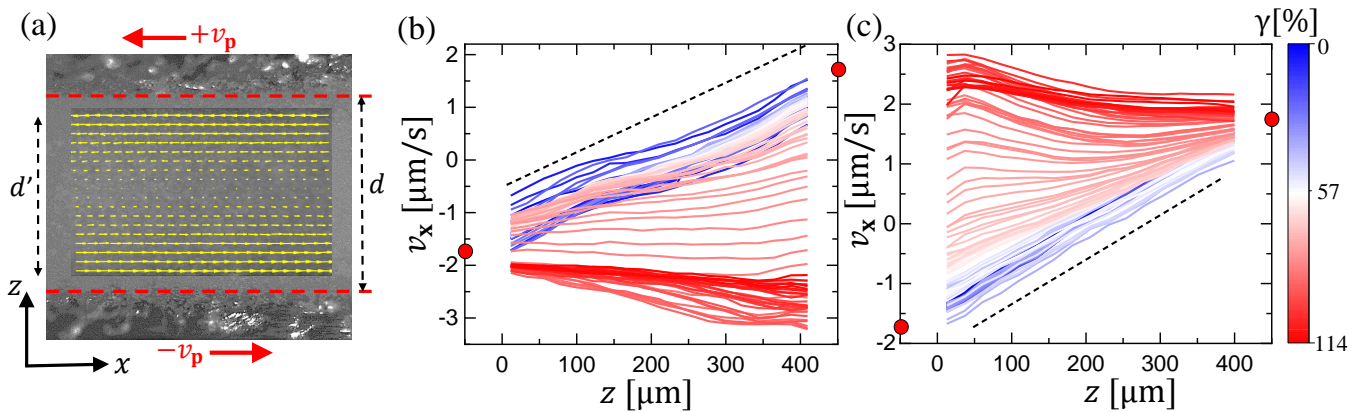


Figure 2: (a) Typical boundary image with superposed velocity profile for the collagen sample seeded with $2.8 \mu\text{m}$ polystyrene particles (1% v/v). d and d' respectively represent the gap between the plates and the sample width used for PIV analysis. $\pm v_p$ denote the plate velocities. (b) and (c) show the velocity profiles obtained from the PIV analysis for $T = 30^\circ\text{C}$ and 25°C , respectively. Color gradient represent increasing applied strain (γ) with a ramp rate of 1%/s. The red dots indicates the plate velocities. The dashed lines represent the velocity profile predicted assuming affine deformations. We see strong non-affine deformation for larger strain values close to yielding. Here, $\phi = 2 \text{ mg/ml}$.

1% (v/v) polystyrene tracer particles ($d = 2.8 \mu\text{m}$) [47] in the collagen samples (Fig. 2(a)) to enhance the scattered intensity required for the PIV measurement. We find that $\sim 1\%$ (v/v) is the minimum amount of tracer particles required to get a fairly uniform distribution of speckle pattern. Freeze fracture SEM images (Materials and Methods) show that the particles have some affinity to stick to the networks (Fig. S4), however, FTIR spectra (Materials and Methods) points out that no chemical bonds between the particles and collagen fibers are formed (Fig. S5). We confirm that introducing such low concentration of tracer particles does not modify the rheological behaviour of collagen networks (Fig. S6). A typical boundary image displaying the speckle pattern with velocity vectors obtained from PIV analysis is shown in Fig. 2(a). The plates are moving with velocities $+v_p$ and $-v_p$ in a counter-rotation configuration giving an applied shear rate $\dot{\gamma} = \frac{2v_p}{d}$, where d is the gap between the plates. Evolution of the spatially-averaged velocity profiles across the gap [$v(z)$ vs z] with increasing strain values are shown in Fig. 2(b) and 2(c) for polymerization temperatures of 30°C and 25°C , respectively. We see that for all strain values $\gamma < \gamma_y$, the profiles remain almost linear, indicating an affine deformation. The average shear rate inside the sample below $\gamma < \gamma_y$ is given by $\frac{2v_0}{d'}$, where $\pm v_0$ indicate the velocities inside the PIV window at $z = 0$ and $z = d'$ (Fig. 2(a)). However, for $\gamma \geq \gamma_y$ the velocity profiles evolve rapidly, in particular, near one of the plate boundaries (Fig. 2(b) and 2(c)) and finally a detachment happens at $\gamma = \gamma_b$ (also see Movie 1). Such evolution of velocity profile indicates strain localization and slippage near the boundary. Beyond the detachment, the shear strain in the network becomes negligible and entire network moves with a constant velocity with the plate remains attached to. Sometimes, the network can also detach from both the plates (Movie 2). Interestingly, for few rare occasions we observe that some part of the network can reattach with the moving plates after the initial detachment giving rise to more complex fracture patterns (data not shown). The boundary near which velocity profiles rapidly evolve and finally sample detachment takes place, randomly varies for different experimental runs and most likely depends on the attachment of the network with the rheometer plates. Such trend is observed for all sample concentrations, temperatures and applied shear rates we consider in the present study. Our observations indicate a close connection between the yielding onset and boundary

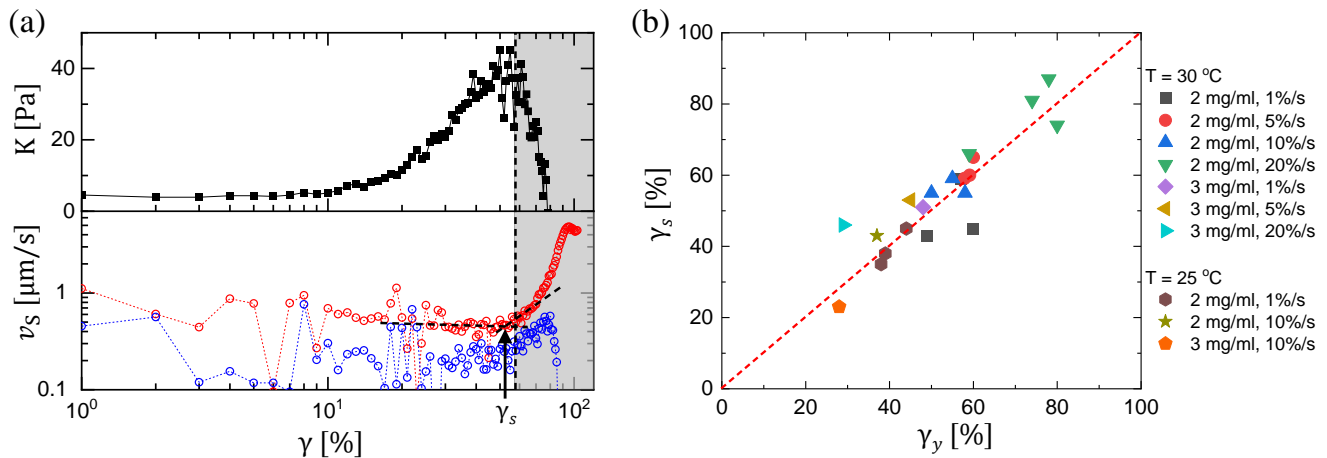


Figure 3: (a) Variation of shear modulus K (top panel) and slip velocity v_s obtained from PIV analysis (bottom panel) for $\phi = 2$ mg/ml and $T = 30^\circ\text{C}$ as a function of applied strain. Slippage between the sample boundary and the rheometr plate show a significant increase beyond the yield strain (γ_y), as shown by the data in the shaded region. Otherwise, such slippage is negligible. We mark the onset strain beyond which the slippage increases (γ_s) by an arrow in the bottom panel. (b) Variation of γ_s as a function of γ_y for a range of sample conditions and strain ramp rates, as marked in the legend. The dashed red-line corresponds to $\gamma_s = \gamma_y$.

dynamics of the collagen network.

To further explore the correlation between the yielding and failure dynamics of the network, we define the slip-velocity $v_s = |v_p - v_0|$ and plot it as a function of applied strain (γ) in Fig. 3(a) for $T = 30^\circ\text{C}$. We find from Fig. 3(a) that v_s remains small as a function of γ till $\gamma = \gamma_y$, for both the top and bottom plates. This indicates that, over a range of strain values, both in the linear and non-linear regime, the slippage between the sample and the plates is not significant. As γ crosses γ_y (indicated by the peak of K), v_s starts to increase rapidly, particularly, for one of the plates and reaches a maximum near $\gamma = \gamma_b$. The maximum value of $v_s \sim 2v_p$, however, in some cases the value of slip-velocity can be even larger due to strong elastic retraction of the network after the rupture. The applied strain value beyond which v_s increases rapidly defines the slip-strain (γ_s), as shown in Fig. 3(a) (bottom panel). To establish the relation of boundary slippage with the yielding behaviour, we plot γ_s as a function of γ_y in Fig. 3(b) for varying sample conditions as well as, strain ramp rates. Remarkably, we observe a strong correlation between γ_s and γ_y , indicating that boundary slippage plays an important role in yielding of collagen networks.

Our observation points out the generality of boundary failure dynamics in governing the yielding behaviour of the networks over a wide range of parameters. Moreover, the appearance of significant boundary slippage only deep inside the strain-stiffening region indicates that such detachment is triggered by internal stresses generated in the system due to strong non-linear deformation of the network. We indeed observe a significant negative normal stress in the system before yielding (Fig. S7). Currently, we do not fully understand why the network failure/rupture always takes place close to the sample boundaries. There can be a possible connection with network rarefaction under non-linear deformation as observed for highly cross-linked actin networks [34]. Such rarefaction results in lower average number of contacts between the filaments close to the boundaries giving rise to a local weakening of the sample. For some cases, we observe a drop in the scattered intensity from the sample near the shearing plates close to yielding (Fig. S8). Such intensity drop near the plates increases further beyond the breaking strain. This observation coupled with the fact

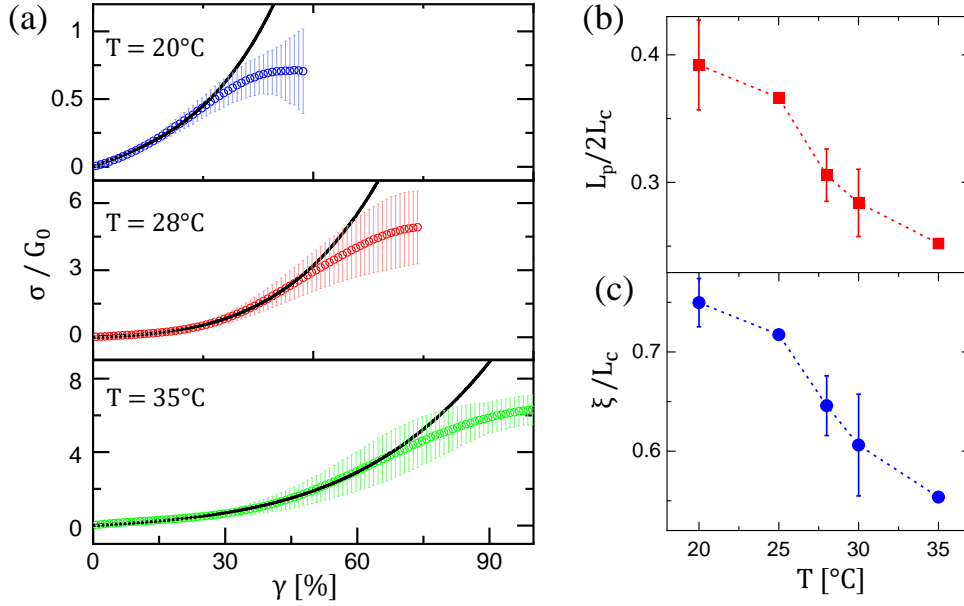


Figure 4: (a) Symbols indicate the variation of normalized stress as a function of applied strain for different polymerization temperatures as shown. Error bars represent the standard deviations obtained from two independent experiments under the same sample condition. Solid lines represent the fits to the 8-chain model as described in the main text. We get very good agreement in all cases upto intermediate strain values, however, significant deviation from the fitted model is observed due to non-affine deformations close to yielding. Variation of reduced persistence length (b) and mesh size (c) as a function of temperature obtained from the fitting. Here, $\phi = 2$ mg/ml.

that tracer particles have an affinity to stick to the collagen fibers (Fig. S4), also supports the local rarefaction picture mentioned earlier. However, more studies are required to confirm such deformation induced network heterogeneity in collagen systems.

Next, we turn to the temperature dependent microscopic network architecture that controls the yielding behaviour in these systems. Although, the mechanical properties of a single biopolymer filament is well described by Worm Like Chain model (WLC) [48], a network formed by many such filaments have random structures that make the derivation of analytical expression for free energy and stress-strain relation extremely complex [28]. To simplify this problem, several lattice-based models have been proposed. These models essentially use the concept of a ‘mesh cell’ or, an elemental volume, such that, the entire sample can be constructed just by 3-D translation of this elemental volume. The main assumption of this model is affine or uniform deformation in the system spanned by the deformation of the ‘mesh cell’. As mentioned earlier, we observe affine deformations over a wide range of strain values below yielding. Thus, such lattice based models should capture the mechanics for collagen networks for $\gamma < \gamma_y$. One such models for the ‘mesh cell’ is *8-chain model*, where the cell is body-centered cubic. Eight chains connect the eight corners of the cube to the center. The mesh size (ξ) of the network is given by the edge-length of the cubic cell. The stress (σ) vs strain (γ) relationship for this network model under simple shear is given by [28],

$$\sigma = \frac{2}{3}nk_B T \gamma a^2 \left[\frac{9}{c\pi[3 - (3 + \gamma^2)a^2]^2} - c\pi^2 \right] \quad (1)$$

where, the parameters $a = \frac{\xi}{L_c}$ and $c = \frac{l_p}{2L_c}$ are the reduced mesh-size and persistence length, respectively. Here, n is the number of entanglement points per unit volume. A dimensionless form of the above equation can be obtained

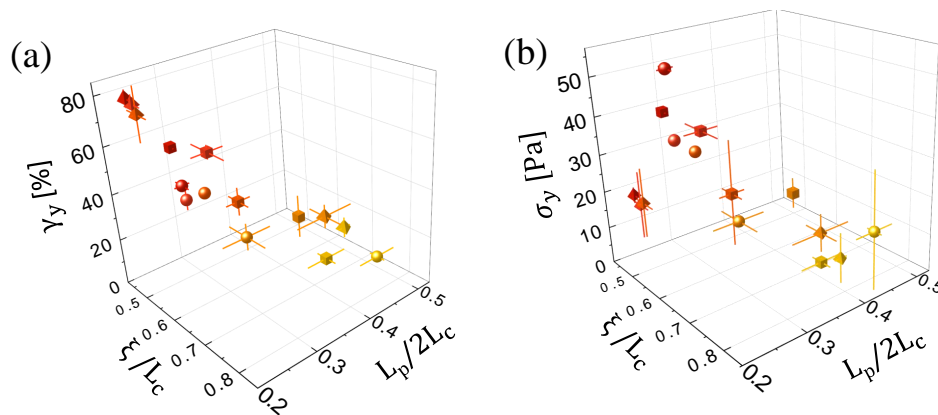


Figure 5: Variation of (a) yield strain (γ_y) and (b) yield stress (σ_y) with reduced persistence length and mesh size. Tetrahedron, cube and sphere shaped symbols correspond to 1 mg/ml, 2 mg/ml and 3 mg/ml collagen concentrations, respectively. Dark to light color represents the decreasing magnitude of γ_y or σ_y . Error bars represent the standard deviations of two independent measurements. Here, $\phi = 2$ mg/ml.

if we divide both sides by the average plateau modulus ($G_0 = \sqrt{G'^2 + G''^2}$) obtained from the frequency sweep data (Fig. S2). We use the above equation to fit σ/G_0 vs γ data obtained experimentally for different temperatures and collagen concentrations. For clarity, we show the fitted data only for $\phi = 2$ mg/ml concentration at three different temperatures in Fig. 4(a). We see very good agreements for strain values $\gamma < \gamma_y$ in all cases. For the fitting initialization, we use n values similar to those obtained in the recent simulations for collagen networks [49] (also see Table of Parameters in S.I.). The parameters $\frac{l_p}{2L_c}$ and $\frac{\xi}{L_c}$ obtained from the fitting are plotted in Fig. 4(b) and (c) as a function of temperature. We find that both of these parameters decrease with increasing temperature. This result also agrees with the variation of filament diameter obtained from the SEM images, where we observe that fibril thickness decreases with increasing temperature (Fig. 1(c)). We should also note that for 8 chain model, it is assumed that each chain is a single collagen filament, however, bundle formation is always present in biopolymers [50]. Also, 8-chain model can not capture the strain softening behaviour at smaller strain values coming predominantly from the filament buckling [9].

We show the dependence of yield strain/stress (γ_y or σ_y) on microscopic network parameters (reduced mesh-size and persistence length) by generalized three-dimensional state diagrams in Fig. 5(a) and (b). The variation of microscopic network architecture is obtained by varying the polymerization temperature (20⁰C - 35⁰C) as well as collagen concentration (1 mg/ml - 3 mg/ml). We see from Fig. 5(a) that with increasing value of reduced mesh size and persistence length γ_y monotonically drops. This is remarkable, since, it indicates that despite of the complex network architecture the yield strain is essentially governed by two microscopic network parameters related to the mesh size and persistence length. Networks with finer fibrils are more resilient. Similar trend is also observed for σ_y (Fig. 5(b)). We note that, although, γ_y shows similar dependence on the reduced mesh size and persistence length for all concentrations, σ_y values for 1 mg/ml collagen networks are much lower. This observation is in line with the results mentioned in [31], where networks with lower connectivity show higher plasticity and larger fracture strain.

III. CONCLUSION

In conclusion, we study the yielding and in-situ strain localization under steady shear in disordered networks of type-I collagen over a range of network architectures obtained by varying the polymerization temperatures and collagen concentrations. Using an unit cell based affine network model we attempt to generalize the yielding behaviour under different sample conditions in terms of microscopic network parameters. For rheology experiments, we use a cone-plate geometry that ensures homogeneous shear-stress field in the sample. This indicates that the observed strain localization does not originate due to any imposed stress heterogeneity in the system. We find that network weakening or yielding starts well below the fracture strain, signifying that yielding is a gradual process in disordered collagen networks. Remarkably, we find a strong correlation between the onset of network slippage and the yield strain for different imposed strain ramp rates, polymerization temperatures and collagen concentrations. Such observation points out the generality of strain localization and boundary failure dynamics in controlling yielding in these systems. Similar to earlier studies [23, 31], we also observe that the networks with higher onset strain values for stiffening (observed for higher polymerization temperatures) also show higher values of the yield and breaking strain as indicated in Fig. 1(e). However, in contrary to the observation of network fracture at random locations [31], we find that boundary slippage leads to detachment/rupture. Since, we image the entire gap between the shearing plates in-situ, our spatial resolution is only $\sim 25 \mu\text{m}$ which is much larger than the network mesh size [36]. This indicates that, although boundary failure predominantly controls the yielding and fracture of the bulk network, local plasticity and fracture over few mesh-sizes can not be ruled out. Furthermore, due to low spatial resolution, we can not confirm whether there is a slippage or, formation of a narrow band of high shear rate close the boundary. To resolve such issues, direct imaging of the network deformation in the flow-gradient plane using fluorescence microscopy or very fast z-scanning (along the gradient direction) of the network using a high speed laser scanning confocal microscope tracking the in-situ deformations, will be an interesting future direction to explore. Nevertheless, due to the roughness of the sand blasted plates, the velocity field very close to the boundary can be quite complex. Our observation of localized network rarefaction correlates well with the strain localization and slippage originating at the sample boundaries. However, more experimental as well as theoretical insights are needed to confirm such mechanism. Our study can provide strategies for delaying network failure and thus help in designing more resilient collagen based scaffolds for various engineering and biomedical applications. We hope that our work will motivate further studies on microscopic mechanism of failure and strain localization in collagen and other biopolymer networks.

IV. AUTHORS CONTRIBUTIONS

S.B., V.V.M. and S.M. designed the research, S.B. and V.V.M. performed the experiment, S.B., R.S. and S.M. performed the data analysis. All the authors contributed in writing the manuscript.

V. ACKNOWLEDGEMENT

S.M. thanks SERB (under DST, Govt. of India) for a Ramanujan Fellowship. We thank Ivo Peters for developing the Matlab codes used for PIV analysis. We also thank Gautam Soni, Pramod Pullarkat, Reji Philip and Ranjini

Bandyopadhyay for allowing us to use their lab/common instrument facilities. We thank K M Yatheendran for help with the SEM imaging and Sachidananda Barik for synthesising the polystyrene particles. We thank Madhu Babu for the help with the FTIR measurements and RRI workshop facility for machining the humidity chamber for the sample.

VI. MATERIAL AND METHODS

A. Chemicals Used:

The collagen hydrogels are synthesised from acid-soluble rat tail collagen Type-I [Conc. 8.70 mg/ml in 0.02 N Acetic acid], (Corning, Bedford, MA). The collagen monomers are polymerized using the phosphate buffered saline (PBS) solution (1X, pH 7.34) prepared by uniform mixing of 2 g of NaCl, 50 mg of KCl, 0.36 g of Na_2HPO_4 and 60 mg of KH_2PO_4 in 250 mL of deionized water, with pH adjusted to 7.4 by adding 0.01 M HCl. The Polystyrene microbeads (PS) are used as the tracer particles are synthesized in the laboratory by a procedure described previously [47].

B. Characterization of Collagen hydrogels:

1. Rheology:

For rheology experiments we use a 2018 made MCR-702 Twin-Drive stress-controlled rheometer (Anton Paar, Graz, Austria). A 25 mm diameter top cone geometry (cone angle: 2°) with a 25 mm diameter parallel bottom plate (both made of stainless steel and both are sandblasted) are used. We mix the collagen monomers of a desired concentration with 1X PBS buffer and transfer the sample on the cold Peltier controlled rheometer bottom plate, immediately. Then the Peltier temperature is increased to the desired value. We polymerize collagen networks between the rheometer plates maintained at a fixed temperature. We also use a humidity chamber to prevent solvent evaporation during the rheology experiments. For in-situ imaging studies, we use a thin layer of 5 cSt silicone oil (Merck) around the sample to prevent solvent evaporation.

2. Freeze-fracture Electron Microscopy:

To probe the collagen network architecture, we carry out SEM imaging using an Ultra Plus Cryo-SEM (Zeiss, Germany) set-up. The collagen hydrogels of different concentrations (1 to 3 mg/ml) are prepared by adding the stock collagen to PBS solution in 1.5 ml centrifuge tubes, followed by a thorough mixing. Different samples of hydrogels were made by varying the polymerization temperature over the range $4^\circ - 35^\circ\text{C}$. Polymerized samples appear translucent under the ambient light. After polymerization, the samples were transferred to the sample holder for freeze-fracture SEM using a micro-pipette, as soon as possible. The sample holder is dipped in liquid nitrogen to freeze the samples instantly. Next, the frozen samples are mounted on the SEM sample stage using carbon tape and are sputter coated with platinum to a thickness of ~ 5 nm using a Polaron SC7620 sputter coater (Watford, UK). After this, SEM images

are recorded. The images are analyzed using ImageJ/Fiji/Matlab software.

3. Fourier Transform Infrared Spectroscopy (FTIR):

A Perkin-Elmer Spectrum 1000 FT-IR spectrometer is used to record the IR spectra of the dried samples of pristine PS, collagen hydrogel and collagen hydrogel with dispersed PS. The spectral positions are typically given in wavenumber (cm^{-1}) unit. The dried samples in very less quantity are mixed with KBr powder in a mortar and then ground well. The mixtures are then made into pellets, and loaded into the sample holder for measurements. Any new chemical interaction between collagen and PS should give rise to new troughs [51–53] for the composite samples as compared to the pristine samples of pure collagen and PS [54]. We find that almost all the troughs in the composite sample match with those for the individual pristine samples (Fig. S5). This indicates that the tracer PS do not form any chemical bonds with the collagen networks.

-
- [1] Cornelis Storm, Jennifer J. Pastore, F. C. MacKintosh, T. C. Lubensky, and Paul A. Janmey. Nonlinear elasticity in biological gels. *Nature*, 435:191–194, May 2005.
 - [2] Paul A. Janmey, Margaret E. McCormick, Sebastian Rammensee, Jennifer L. Leight, Penelope C. Georges, and Fred C. MacKintosh. Negative normal stress in semiflexible biopolymer gels. *Nat. Mater.*, 6:48–51, Jan 2007.
 - [3] Ovijit Chaudhuri, Sapun H. Parekh, and Daniel A. Fletcher. Reversible stress softening of actin networks. *Nature*, 445:295–298, Jan 2007.
 - [4] Albert James Licup, Stefan Münster, Abhinav Sharma, Michael Sheinman, Louise M. Jawerth, Ben Fabry, David A. Weitz, and Fred C. MacKintosh. Stress controls the mechanics of collagen networks. *Proc. Natl. Acad. Sci. U.S.A.*, 112(31):9573–9578, Aug 2015.
 - [5] Andrew M. Stein, David A. Vader, David A. Weitz, and Leonard M. Sander. The micromechanics of three-dimensional collagen-I gels. *Complexity*, 16(4):22–28, Mar/Apr 2011.
 - [6] Peter Fratzl, Klaus Misof, Ivo Zizak, Gert Rapp, Heinz Amenitsch, and Sigrid Bernstorff. Fibrillar Structure and Mechanical Properties of Collagen. *J. Struct. Biol.*, 122(1):119–122, Jan 1998.
 - [7] M. L. Gardel, J. H. Shin, F. C. MacKintosh, L. Mahadevan, P. Matsudaira, and D. A. Weitz. Elastic Behavior of Cross-Linked and Bundled Actin Networks. *Science*, 304(5675):1301–1305, May 2004.
 - [8] C. P. Broedersz and F. C. MacKintosh. Modeling semiflexible polymer networks. *Rev. Mod. Phys.*, 86(3):995–1036, Jul 2014.
 - [9] P. R. Onck, T. Koeman, T. van Dillen, and E. van der Giessen. Alternative Explanation of Stiffening in Cross-Linked Semiflexible Networks. *Phys. Rev. Lett.*, 95(17):178102, Oct 2005.
 - [10] Clifford P. Brangwynne, Gijsje H. Koenderink, Ed Barry, Zvonimir Dogic, Frederick C. MacKintosh, and David A. Weitz. Bending Dynamics of Fluctuating Biopolymers Probed by Automated High-Resolution Filament Tracking. *Biophys. J.*, 93(1):346–359, Jul 2007.
 - [11] Bruce Alberts, Alexander Johnson, Julian Lewis, Martin Raff, Keith Roberts, and Peter Walter. *Molecular Biology of the Cell*. Garland Science, New York, NY, USA, 2002.
 - [12] Tania Rozario and Douglas W. DeSimone. The extracellular matrix in development and morphogenesis: A dynamic view. *Dev. Biol.*, 341(1):126–140, May 2010.

- [13] Janna K. Mouw, Guanqing Ou, and Valerie M. Weaver. Extracellular matrix assembly: a multiscale deconstruction. *Nat. Rev. Mol. Cell Biol.*, 15:771–785, Nov 2014.
- [14] Qi Wen, Anindita Basu, Paul A. Janmey, and A. G. Yodh. Non-affine deformations in polymer hydrogels. *Soft Matter*, 8(31):8039, Jan 2012.
- [15] Matthew W. Conklin, Jens C. Eickhoff, Kristin M. Riching, Carolyn A. Pehlke, Kevin W. Eliceiri, Paolo P. Provenzano, Andreas Friedl, and Patricia J. Keely. Aligned Collagen Is a Prognostic Signature for Survival in Human Breast Carcinoma. *Am. J. Pathol.*, 178(3):1221, Mar 2011.
- [16] Cameron Walker, Elijah Mojares, and Armando Del Río Hernández. Role of Extracellular Matrix in Development and Cancer Progression. *Int. J. Mol. Sci.*, 19(10):3028., Oct 2018.
- [17] Arti Vashist, Atul Vashist, Y. K. Gupta, and Sharif Ahmad. Recent advances in hydrogel based drug delivery systems for the human body. *J. Mater. Chem. B*, 2(2):147–166, Oct 2013.
- [18] Jos Malda, Jetze Visser, Ferry P. Melchels, Tomasz Jüngst, Wim E. Hennink, Wouter J. A. Dhert, Jürgen Groll, and Dietmar W. Hutmacher. 25th Anniversary Article: Engineering Hydrogels for Biofabrication. *Adv. Mater.*, 25(36):5011–5028, Sep 2013.
- [19] Jiranuwat Sapudom, Stefan Rubner, Steve Martin, Tony Kurth, Stefanie Riedel, Claudia T. Mierke, and Tilo Pompe. The phenotype of cancer cell invasion controlled by fibril diameter and pore size of 3D collagen networks. *Biomaterials*, 52:367–75, Jun 2015.
- [20] Sungmin Nam, Kenneth H. Hu, Manish J. Butte, and Ovijit Chaudhuri. Strain-enhanced stress relaxation impacts nonlinear elasticity in collagen gels. *Proc. Natl. Acad. Sci. U.S.A.*, 113(20):5492–5497, May 2016.
- [21] Ya-li Yang and Laura J. Kaufman. Rheology and Confocal Reflectance Microscopy as Probes of Mechanical Properties and Structure during Collagen and Collagen/Hyaluronan Self-Assembly. *Biophys. J.*, 96(4):1566–1585, Feb 2009.
- [22] David Vader, Alexandre Kabla, David Weitz, and Lakshminarayana Mahadevan. Strain-induced alignment in collagen gels. *PLoS ONE*, 4:1–12, Jun 2009.
- [23] Karin A. Jansen, Albert J. Licup, Abhinav Sharma, Robbie Rens, Fred C. MacKintosh, and Gijsje H. Koenderink. The Role of Network Architecture in Collagen Mechanics. *Biophys. J.*, 114(11):2665–2678, Jun 2018.
- [24] Stéphanie Motte and Laura J. Kaufman. Strain stiffening in collagen I networks. *Biopolymers*, 99(1):35–46, Jan 2013.
- [25] J. Clerk Maxwell. L. On the calculation of the equilibrium and stiffness of frames. *London, Edinburgh, and Dublin Philosophical Magazine and Journal of Science*, 27(182):294–299, Apr 1864.
- [26] Yuval Mulla, F. C. MacKintosh, and Gijsje H. Koenderink. Origin of Slow Stress Relaxation in the Cytoskeleton. *Phys. Rev. Lett.*, 122(21):218102, May 2019.
- [27] A. Sharma, A. J. Licup, K. A. Jansen, R. Rens, M. Sheinman, G. H. Koenderink, and F. C. MacKintosh. Strain-controlled criticality governs the nonlinear mechanics of fibre networks. *Nat. Phys.*, 12:584–587, Jun 2016.
- [28] Fanlong Meng and Eugene M. Terentjev. Nonlinear elasticity of semiflexible filament networks. *Soft Matter*, 12(32):6749–6756, Aug 2016.
- [29] Jeffrey S. Palmer and Mary C. Boyce. Constitutive modeling of the stress–strain behavior of F-actin filament networks. *Acta Biomater.*, 4(3):597–612, May 2008.
- [30] Khanh-Hoa Tran-Ba, Daniel J. Lee, Jieling Zhu, Keewook Paeng, and Laura J. Kaufman. Confocal Rheology Probes the Structure and Mechanics of Collagen through the Sol-Gel Transition. *Biophys. J.*, 113(8):1882–1892, Oct 2017.
- [31] Federica Burla, Simone Dussi, Cristina Martinez-Torres, Justin Tauber, Jasper van der Gucht, and Gijsje H. Koenderink. Connectivity and plasticity determine collagen network fracture. *Proc. Natl. Acad. Sci. U.S.A.*, 117(15):8326–8334, Apr 2020.
- [32] Richard C. Arevalo, Pramukta Kumar, Jeffrey S. Urbach, and Daniel L. Blair. Stress Heterogeneities in Sheared Type-I Collagen Networks Revealed by Boundary Stress Microscopy. *PLoS One*, 10(3):e0118021, Mar 2015.

- [33] Sayantan Majumdar, Louis C. Foucard, Alex J. Levine, and Margaret L. Gardel. Mechanical hysteresis in actin networks. *Soft Matter*, 14(11):2052–2058, Mar 2018.
- [34] K. M. Schmoller, P. Fernández, R. C. Arevalo, D. L. Blair, and A. R. Bausch. Cyclic hardening in bundled actin networks. *Nat. Commun.*, 1(134):1–8, Dec 2010.
- [35] Stefan Münster, Louise M. Jawerth, Beverly A. Leslie, Jeffrey I. Weitz, Ben Fabry, and David A. Weitz. Strain history dependence of the nonlinear stress response of fibrin and collagen networks. *Proc. Natl. Acad. Sci. U.S.A.*, 110(30):12197–12202, Jul 2013.
- [36] Richard C. Arevalo, Jeffrey S. Urbach, and Daniel L. Blair. Size-Dependent Rheology of Type-I Collagen Networks. *Biophys. J.*, 99(8):L65–L67, Oct 2010.
- [37] Alfonso Gautieri, Simone Vesentini, Alberto Redaelli, and Markus J. Buehler. Hierarchical Structure and Nanomechanics of Collagen Microfibrils from the Atomistic Scale Up. *Nano Lett.*, 11(2):757–766, Feb 2011.
- [38] H. Utiyama, K. Sakato, K. Ikehara, T. Setsuiye, and M. Kurata. Flexibility of tropocollagen from sedimentation and viscosity. *Biopolymers*, 12(1):53–64, Jan 1973.
- [39] Christopher B. Raub, Vinod Suresh, Tatiana Krasieva, Julia Lyubovitsky, Justin D. Mih, Andrew J. Putnam, Bruce J. Tromberg, and Steven C. George. Noninvasive Assessment of Collagen Gel Microstructure and Mechanics Using Multiphoton Microscopy. *Biophys. J.*, 92(6):2212–2222, Mar 2007.
- [40] Katarina Wolf, Mariska Te Lindert, Marina Krause, Stephanie Alexander, Joost Te Riet, Amanda L. Willis, Robert M. Hoffman, Carl G. Figdor, Stephen J. Weiss, and Peter Friedl. Physical limits of cell migration: Control by ECM space and nuclear deformation and tuning by proteolysis and traction force. *J. Cell Biol.*, 201(7):1069, Jun 2013.
- [41] Yu-Jer Hwang and Julia G. Lyubovitsky. Collagen hydrogel characterization: multi-scale and multi-modality approach. *Anal. Methods*, 3(3):529–536, Mar 2011.
- [42] Christopher B. Raub, Jay Unruh, Vinod Suresh, Tatiana Krasieva, Tore Lindmo, Enrico Gratton, Bruce J. Tromberg, and Steven C. George. Image correlation spectroscopy of multiphoton images correlates with collagen mechanical properties. *Biophys. J.*, 94(6):2361 – 2373, Mar 2008.
- [43] Blayne A. Roeder, Klod Kokini, Jennifer E. Sturgis, J. Paul Robinson, and Sherry L. Voytik-Harbin. Tensile mechanical properties of three-dimensional type I collagen extracellular matrices with varied microstructure. *J. Biomech. Eng.*, 124(2):214–222, Apr 2002.
- [44] J. Robin Harris and Andreas Reiber. Influence of saline and pH on collagen type I fibrillogenesis in vitro: Fibril polymorphism and colloidal gold labelling. *Micron*, 38(5):513–521, Jul 2007.
- [45] Xuye Lang and Julia G. Lyubovitsky. Structural dependency of collagen fibers on ion types revealed by in situ second harmonic generation (SHG) imaging method. *Anal. Methods*, 7(5):1680–1690, Feb 2015.
- [46] Ya li Yang, Lindsay M. Leone, and Laura J. Kaufman. Elastic moduli of collagen gels can be predicted from two-dimensional confocal microscopy. *Biophys. J.*, 97(7):2051 – 2060, Oct 2009.
- [47] Subhransu Dhar, Sebanti Chattopadhyay, and Sayantan Majumdar. Signature of jamming under steady shear in dense particulate suspensions. *Journal of Physics: Condensed Matter*, 32(12):124002, Dec 2019.
- [48] O. Kratky and G. Porod. Röntgenuntersuchung gelöster Fadenmoleküle. *Recl. Trav. Chim. Pays-Bas*, 68(12):1106–1122, Jan 1949.
- [49] Clara Valero, Hippolyte Amaveda, Mario Mora, and Jose Manuel García-Aznar. Combined experimental and computational characterization of crosslinked collagen-based hydrogels. *PLoS One*, 13(4):e0195820, Apr 2018.
- [50] Jörg Schnauß, Tina Händler, and Josef A. Käs. Semiflexible Biopolymers in Bundled Arrangements. *Polymers*, 8(8):274, Jul 2016.
- [51] K. J. Payne and A. Veis. Fourier transform ir spectroscopy of collagen and gelatin solutions: Deconvolution of the amide i band for conformational studies. *Biopolymers*, 27(11):1749–1760, Nov 1988.

- [52] Benedicto de Campos Vidal and Maria Luiza S. Mello. Collagen type i amide i band infrared spectroscopy. *Micron*, 42(3):283 – 289, Apr 2011.
- [53] Karima Belbachir, Razia Noreen, Gilles Gousspillou, and Cyril Petibois. Collagen types analysis and differentiation by FTIR spectroscopy. *Anal. Bioanal.Chem.*, 395(3):829–837, Oct 2009.
- [54] JunFei Fang, YiMin Xuan, and Qiang Li. Preparation of polystyrene spheres in different particle sizes and assembly of the PS colloidal crystals. *Sci. China Technol. Sci.*, 53(11):3088–3093, Nov 2010.

Supplementary Information: Strain localization and yielding dynamics in disordered collagen networks

Movie Descriptions

Movie1: In this movie, we show the in-situ deformation of the sample surface in flow-gradient plane correlating with stress vs strain response of collagen network (2 mg/ml) seeded with 1% (v/v) PS. The applied strain ramp rate is 1%/s. The images are captured using a digital camera (Lumenera) fitted with a 5X long working distance objective (Mitutoyo) at a frame rate of 1 Hz with a resolution of 1200 X 1800 (pixel)². The images are then cropped and compressed such that the spatial resolution is $\sim 1.4 \mu\text{m}/\text{pixel}$. The movie is sped up 14 times as compared to the real time. As mentioned in the main text, we see that network slippage with one of the shearing plates (here, top plate) appears well before the peak stress/breaking stress is reached. The onset of such slippage correlates well with the yield strain of the network (as indicated in the movie). Beyond the peak stress, the detachment (characterized by an elastic retraction of the whole network) takes place from the top plate. The drop in scattered intensity near the top plate close to the yield strain indicates network rarefaction (also see Fig. S8 and the main text) before detachment.

Movie2: In this movie, we show the in-situ deformation of collagen network (2 mg/ml) seeded with 1% (v/v) PS for an applied strain ramp rate of 10%/s. The movie is sped up 1.4 times as compared to the real time. Here also, we find similar correlation of the boundary dynamics with the yield and breaking strains of the network (data not shown). Interestingly, as opposed to Movie1, the network detachment happens from both the plates in this case. Also, we see a clear signature of network rarefaction (drop in scattered intensity) near the shearing boundaries close to yielding (also see Fig. S8). Beyond the network breakage/rupture from both the plates, a clear signature of network contraction away from the plates is seen.

Table of parameters

Parameters obtained from the 8-chain model fitting for three different collagen concentrations.

$\phi = 1\text{mg/ml}$

Temperature ($^{\circ}\text{C}$)	$nk_B T (\text{Jm}^{-3})$	$\frac{l_p}{2L_c}$	$\frac{\xi}{L_c}$
20	80	0.421	0.760
25	180	0.400	0.738
30	200	0.235	0.488
35	270	0.234	0.479
37	380	0.229	0.470

$\phi = 2\text{mg/ml}$

Temperature ($^{\circ}\text{C}$)	$nk_B T (\text{Jm}^{-3})$	$\frac{l_p}{2L_c}$	$\frac{\xi}{L_c}$
20	100	0.390	0.750
25	335	0.366	0.717
28	350	0.306	0.646
30	370	0.284	0.606
35	470	0.252	0.554

$\phi = 3\text{mg/ml}$

Temperature ($^{\circ}\text{C}$)	$nk_B T (\text{Jm}^{-3})$	$\frac{l_p}{2L_c}$	$\frac{\xi}{L_c}$
20	300	0.463	0.790
25	350	0.308	0.658
28	380	0.273	0.607
30	420	0.255	0.579
35	500	0.253	0.574

Supplementary figures

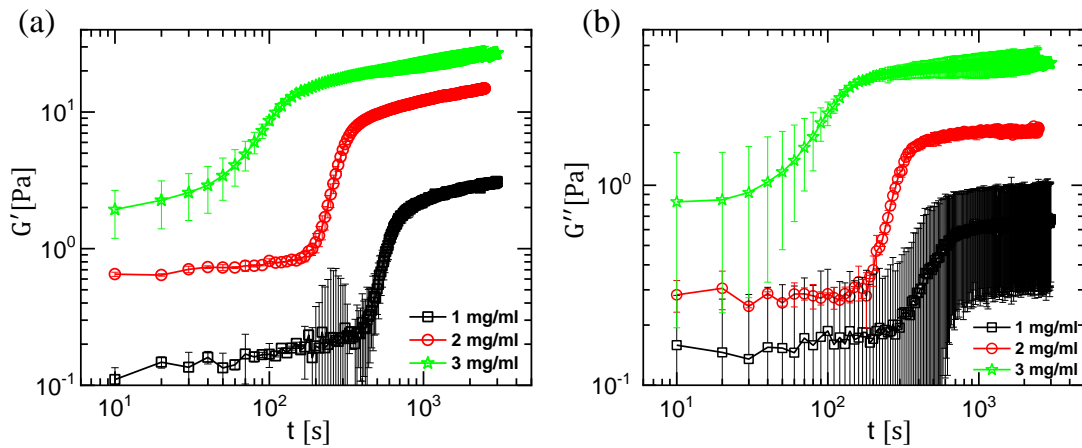


Figure S1: Variation of storage (G' , panel (a)) and loss (G'' , panel (b)) moduli as a function of time during the polymerization of collagen networks. The applied oscillatory strain amplitude is 2% and frequency is 0.5 Hz. As indicated, different symbols represent different concentrations of collagen. The plateau reached after the jump in G' or G'' values represents the polymerized state of the network. The error bars are the standard deviations of two independent measurements under the same condition. Here, polymerization temperature (T) is 25°C in all cases.

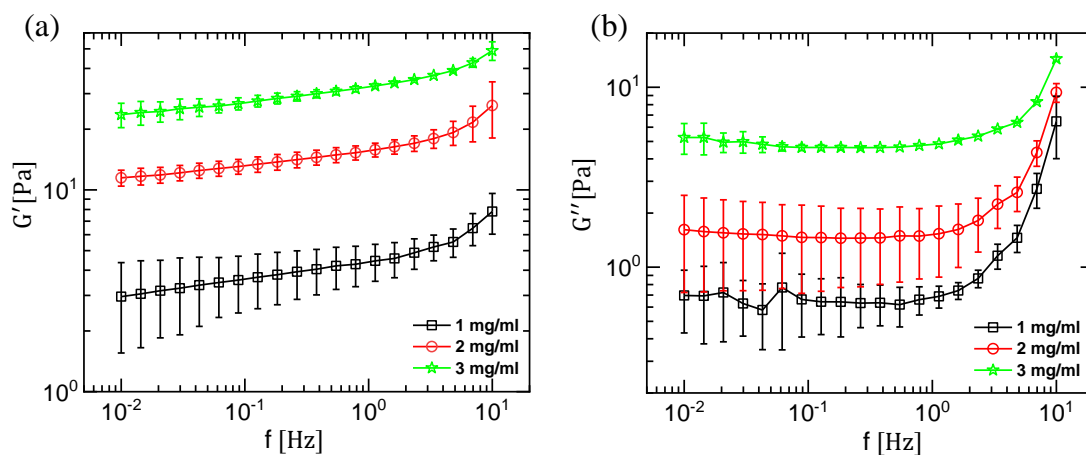


Figure S2: Frequency dependent storage (G' , panel (a)) and loss (G'' , panel (b)) moduli for polymerized collagen networks. The applied oscillatory strain amplitude is 2%. Different symbols represent different concentrations of collagen. T = 25°C. The error bars are the standard deviations of two independent measurements under the same condition. We see that, $G' \gg G''$ over the entire range of frequencies probed.

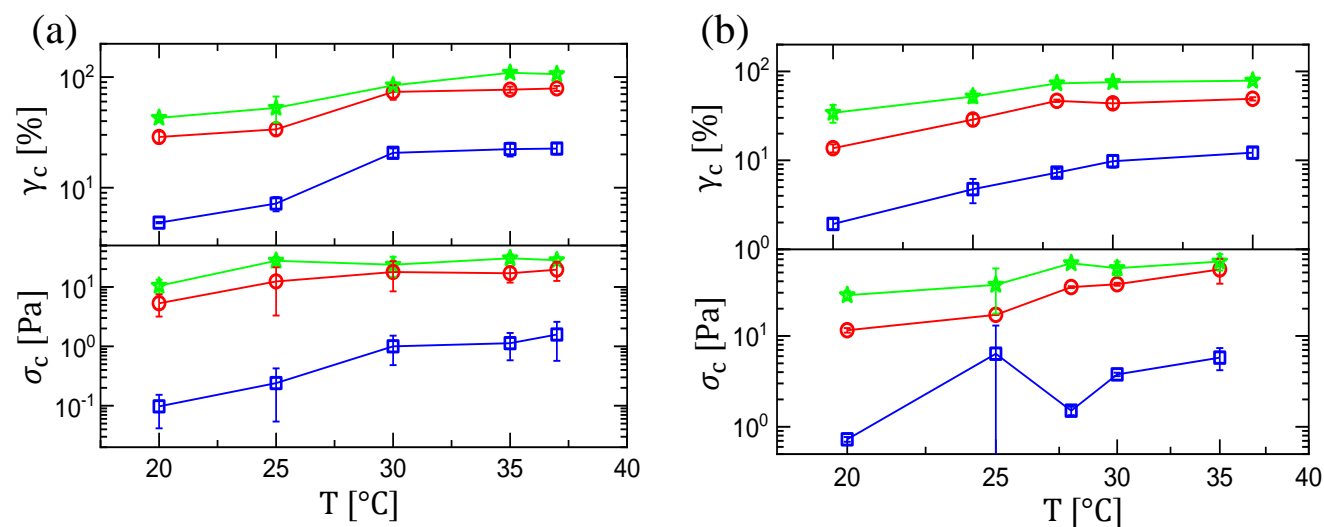


Figure S3: Variation of critical stress and strain values with polymerization temperature for collagen networks. Collagen concentration, $\phi = 1$ mg/ml (panel (a)) and $\phi = 3$ mg/ml (panel (b)). Here, squares represent onset strain/stress, circles represent yield strain/stress and stars represent breaking strain/stress. The error bars are the standard deviations of two independent measurements under the same condition.

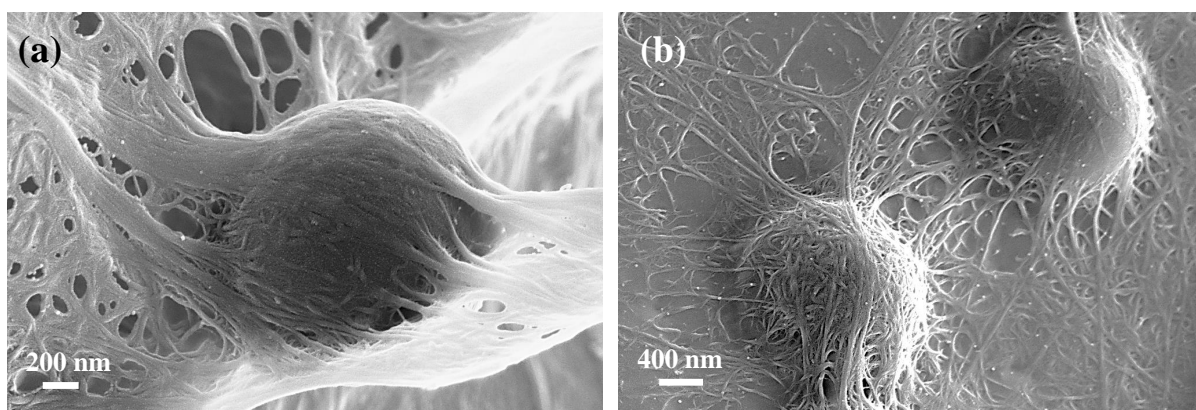


Figure S4: Freeze fracture SEM image of collagen network ($\phi = 2$ mg/ml) seeded with 1% PS of mean diameter of $2.8 \mu\text{m}$. The collagen fibrils seem to have some affinity to stick to the PS surface.

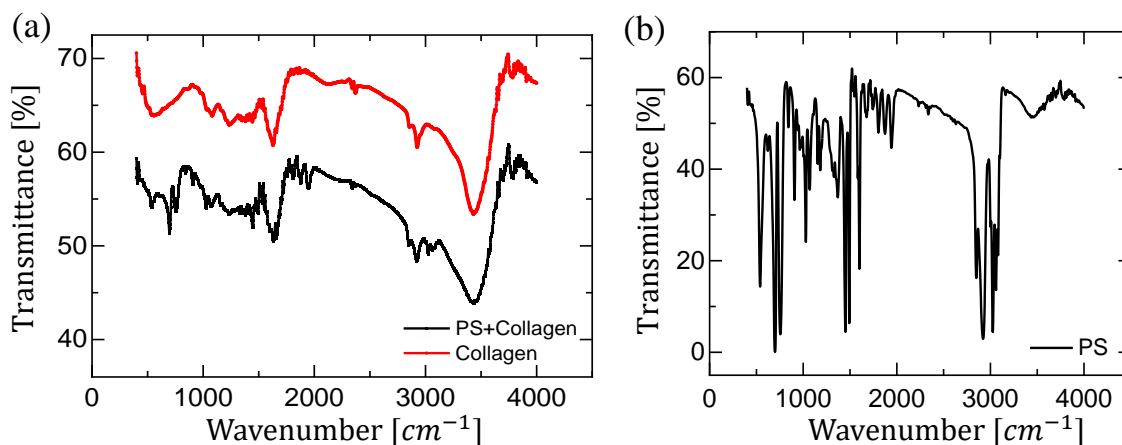


Figure S5: FTIR spectra of pure collagen (shown by the red line in (a)) and collagen mixed with 1% PS (shown by the black line in (a)). FTIR spectrum for only PS particles are shown in (b). As indicated in (a), troughs shown in both the spectra (pure collagen and collagen + PS) are very similar. This indicates that there are no chemical bonding interactions between collagen and PS.

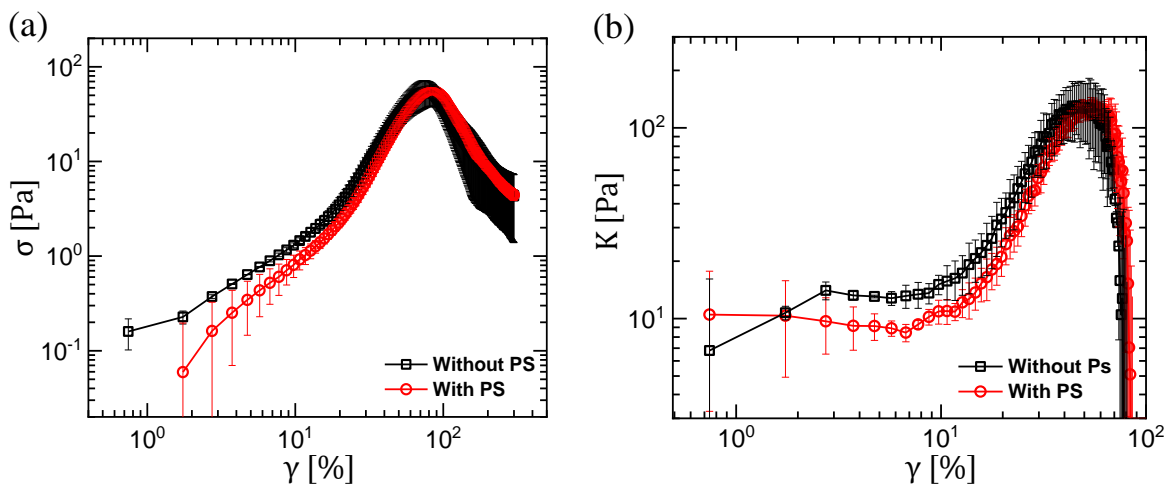


Figure S6: Comparison of network response with and without added PS (1%). We see that stress (σ , panel (a)) and differential shear modulus (K , panel (b)) show very similar behaviour with applied strain (γ) for both the cases. The error bars are the standard deviations of two independent measurements under the same condition. Here, $\phi = 2$ mg/ml and $T = 30^\circ C$.

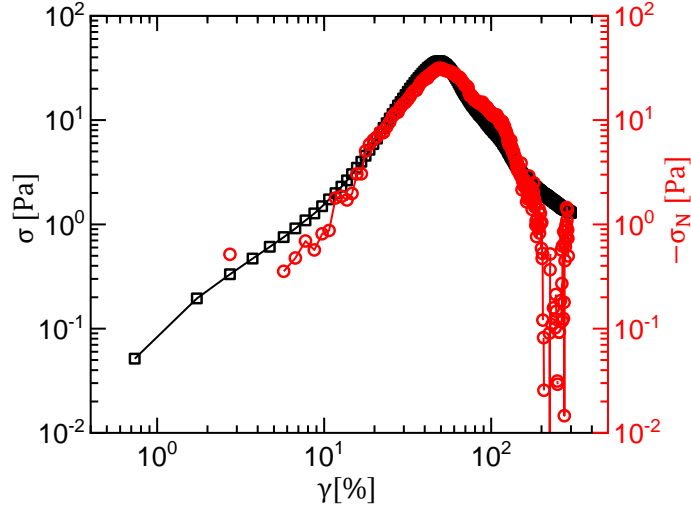


Figure S7: Typical variation of shear stress (σ , shown by the black squares) and negative normal stress (σ_N , shown by the red circles) as a function of applied strain γ for collagen network with $\phi = 2$ mg/ml and $T = 25^\circ\text{C}$. We see that significant negative normal stress (comparable to the shear stress) develops in the network in the strain stiffening regime and reaches a maximum near the yielding.

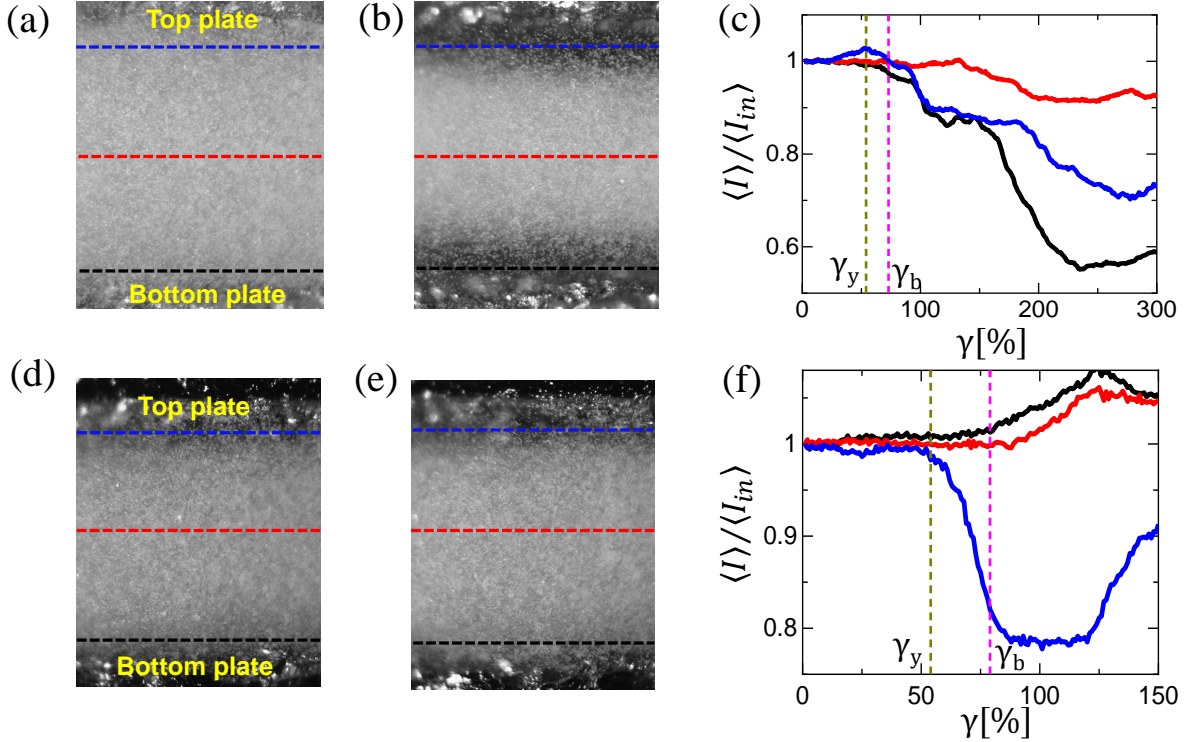


Figure S8: Panels (a), (b), (d) and (e) show typical boundary images of the sample with dashed horizontal lines parallel to the plates indicating the positions where the average intensity (normalized by the initial intensity) as a function of applied strain (γ) are calculated as shown in (c) and (f). Positions near the top and bottom plates indicated by blue and black lines, respectively. Red line indicates a position near the midway between the plates. (a), (b), (c) correspond to a strain ramp rate of 10%/s and (d), (e), (f) correspond to 1%/s. For both ramp rates, the intensity near both the plates (c) or, one of the plates (f) drops significantly beyond the yield (γ_y) and the breaking (γ_b) strains as indicated. Panels (a) and (d) correspond to the initial unstrained state ($\gamma = 0$) of the sample, whereas, (b) and (e) represent that after the network rupture. The drop in scattered intensity near yielding indicates network rarefaction leading to detachment. Here, $\phi = 2$ mg/ml and $T = 30^\circ\text{C}$.